

## Article

# Modelling and Molecular Dynamics Predict the Structure and Interactions of the Glycine Receptor Intracellular Domain

James R. E. Thompson, Christopher A. Beaudoin and Sarah C. R. Lummis \*

Department of Biochemistry, University of Cambridge, Cambridge CB2 1QW, UK

\* Correspondence: sl120@cam.ac.uk; Tel.: +44-1223-765950; Fax: +44-1223-333345

**Abstract:** Glycine receptors (GlyRs) are glycine-gated inhibitory pentameric ligand-gated ion channels composed of  $\alpha$  or  $\alpha + \beta$  subunits. A number of structures of these proteins have been reported, but to date, these have only revealed details of the extracellular and transmembrane domains, with the intracellular domain (ICD) remaining uncharacterised due to its high flexibility. The ICD is a region that can modulate function in addition to being critical for receptor localisation and clustering via proteins such as gephyrin. Here, we use modelling and molecular dynamics (MD) to reveal details of the ICDs of both homomeric and heteromeric GlyR. At their N and C ends, both the  $\alpha$  and  $\beta$  subunit ICDs have short helices, which are major sites of stabilising interactions; there is a large flexible loop between them capable of forming transient secondary structures. The  $\alpha$  subunit can affect the  $\beta$  subunit ICD structure, which is more flexible in a  $4\alpha_2:1\beta$  than in a  $4\alpha_1:1\beta$  GlyR. We also explore the effects of gephyrin binding by creating GlyR models bound to the gephyrin E domain; MD simulations suggest these are more stable than the unbound forms, and again there are  $\alpha$  subunit-dependent differences, despite the fact the gephyrin binds to the  $\beta$  subunit. The bound models also suggest that gephyrin causes compaction of the ICD. Overall, the data expand our knowledge of this important receptor protein and in particular clarify features of the underexplored ICD.

**Keywords:** pentameric ligand-gated ion channel Cys-loop receptor; gephyrin; binding site



**Citation:** Thompson, J.R.E.; Beaudoin, C.A.; Lummis, S.C.R. Modelling and Molecular Dynamics Predict the Structure and Interactions of the Glycine Receptor Intracellular Domain. *Biomolecules* **2023**, *13*, 1757. <https://doi.org/10.3390/biom13121757>

Academic Editor: Brigita Urbanc

Received: 31 August 2023

Revised: 28 November 2023

Accepted: 1 December 2023

Published: 7 December 2023



**Copyright:** © 2023 by the authors. Licensee MDPI, Basel, Switzerland. This article is an open access article distributed under the terms and conditions of the Creative Commons Attribution (CC BY) license (<https://creativecommons.org/licenses/by/4.0/>).

## 1. Introduction

Glycine receptors (GlyRs) are members of the Cys-loop superfamily of ligand-gated ion channels (also known as pentameric ligand-gated ion channel or pLGICs), which includes nicotinic acetylcholine receptors (nAChRs), 5-HT<sub>3</sub> receptors (5-HT<sub>3</sub>Rs), and GABA<sub>A</sub> receptors (GABA<sub>A</sub>Rs) [1,2]. The superfamily members have low sequence homology, but they share a homologous structure in which five subunits pseudo-symmetrically surround a central ion-conducting pore. GlyRs mediate neurotransmission in the brain stem and spinal cord through a glycine-dependent chloride ion influx, causing inhibitory hyperpolarisation in postsynaptic cells [1]. In humans, GlyRs mainly function in pain perception and motor control, with their dysregulation being associated with a range of disorders, including autism and temporal lobe epilepsy [3–5]. Mutant GlyRs, however, are most notable for causing human channelopathy hyperekplexia or startle disease.

There are four GlyR $\alpha$  subunit genes (*glra1-4*) and one GlyR $\beta$  subunit gene (*glrb*); however, in humans, *glra4* functions as a pseudogene due to the introduction of a premature stop codon. GlyRs consist of  $\alpha$  or  $\alpha$  and  $\beta$  subunits forming either homomeric  $\alpha$  receptors or heteromeric  $\alpha\beta$  receptors; current evidence suggests an invariant  $4\alpha:1\beta$  heteromeric stoichiometry for both  $\alpha_1\beta$  GlyRs and  $\alpha_2\beta$  GlyRs [6,7]. The presence of  $\beta$  subunits affects pharmacological properties such as picrotoxin efficacy [1], but their major role may be in the binding of intracellular proteins, which control receptor clustering and localisation. The best-studied of these is gephyrin, a 93kDa scaffolding protein which connects GlyRs to the cytoskeleton [8,9]. Gephyrin binds to GlyR  $\beta$  subunits; molecular details of this have been revealed from a crystal structure of a 15-amino-acid GlyR  $\beta$  subunit peptide bound to the C-terminal domain of gephyrin (GephE) [10].

The GlyR, like other pLGICs, has three major domains: the extracellular (ECD), transmembrane (TM), and intracellular (ICD) domain. Many structural studies, however, start by removing the ICD, which is poorly conserved (Figure 1) and flexible. The receptor does function in heterologous systems without this domain, but in vivo it is important as it can modulate a range of characteristics including channel conductance, desensitisation, agonist efficacy, and receptor clustering [8,11,12]. It is also the site of interaction of a range of intracellular proteins, some of which affect assembly and function, while others may regulate downstream signalling pathways. An understanding of the ICD’s structure and function is therefore pivotal in understanding the physiological roles and regulation of GlyRs. This does, however, present a problem, as determining the structure and interactions of large flexible regions of proteins is still very challenging. There has to date only been one structural study on the ICD of a pLGIC—the homomeric  $\alpha_7$  nAChR—using nuclear magnetic resonance (NMR) and electron spin resonance experiments combined with Rosetta computations. There are still some problems with these methods of structure determination, in particular the receptor is too large for solution NMR, and thus the study required the use of a suitable smaller construct, which may not fully recapitulate the organisation of the protein in the complete receptor. Nevertheless, these data do provide an experimentally based structure that can be used as a template in protein prediction programs. Some of these programs are highly accurate, much more so than when the acetylcholine-binding protein (AChBP, a pLGIC ECD analogue whose structure was published many years before the structures of any complete receptors were known) was used to model pLGIC ECDs, and even then, relatively imperfect programs provided many useful insights.

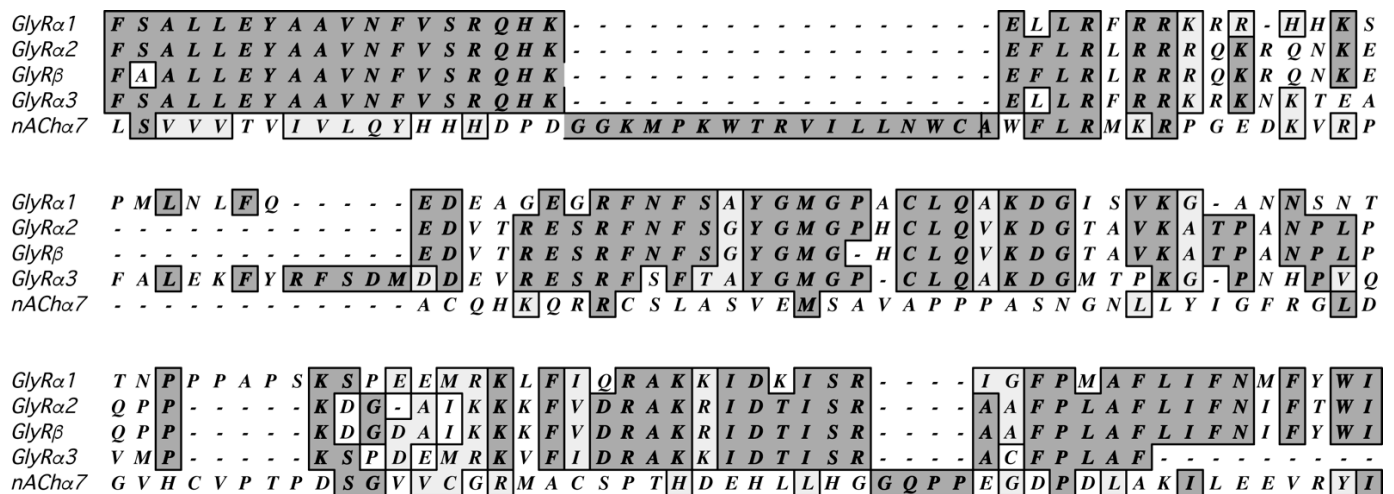


**Figure 1.** A Clustal Omega sequence alignment of the ICD reveals low sequence similarity between human GlyR subunits and also between other human pLGIC subunits, such as the  $\alpha_7$  nAChR subunit. Residue identity and lone residues are shown in dark grey, and residues with similar chemical properties are shown in light grey. Residue numbers are GlyR $\alpha_1$ : 299–444;  $\alpha_2$ : 306–439;  $\beta$ : 329–438;  $\alpha_3$ : 328–430; nAChR $\alpha_7$ : 318–469.

Given the importance of the ICD, we wished to explore the structure, stability, flexibility, and interactions of this domain in the GlyR, a pLGIC related to the  $\alpha_7$ nAChR but which has very different physiological roles. This protein has the advantage of having a relatively well-studied intracellular binding protein—gephyrin—whose C-terminal domain structure, when bound to a GlyR peptide, has been published [10]. However, that study could not determine what affect binding has on protein structure, and indeed, the only method currently available to obtain such information is molecular dynamics experiments. Therefore, here we describe how we used homology-based modelling and molecular dynamics (MD) to create and explore five models of the glycine receptor: one homomeric receptor (5 $\alpha_1$ ), two heteromeric receptors (4 $\alpha_1$ :1 $\beta$  and 4 $\alpha_2$ :1 $\beta$ ), and two GephE-bound receptors

( $4\alpha_1:1\beta$ -GephE and  $4\alpha_2:1\beta$ -GephE). Using these models, we compared the structure and characteristics of the previously undefined GlyR ICD.

## 2. Materials and Methods

### 2.1. Model Generation

We used ProtCHOIR [13] and MODELLER [14] to generate the GlyR models using the crystal structure of the  $\alpha_3$  homomeric human glycine receptor [15] as a template for the  $\alpha$  subunits (PDB ID: 5TIN). Signal peptides were removed from structural templates and alignments were performed with MAFFT v 7.515 [16]. As there are not yet any human heteromeric GlyR structures or any GlyR ICDs, three templates were used for each heteromeric model: the Cryo-EM structure of the ECD and TMD (PDB IDs: 7MLY and 5BKF), a ProtCHOIR-generated homomeric  $\alpha_1$  or  $\alpha_2$  receptor, and an AlphaFold [17]-predicted GlyR  $\beta$  subunit. All models were in the closed state. The gephyrin-bound models  $4\alpha_1:1\beta$ -GephE and  $4\alpha_2:1\beta$ -GephE were generated using the GlyR models and the C-terminal GephE domain bound to a GlyR  $\beta$  subunit peptide (PDB ID: 4PD1) using MODELLER and Z-DOCK—a Fast Fourier Transform algorithm which uses electrostatics, desolvation, and shape complementarity to dock rigid bodies [18]. The successful docked models were selected after a qualitative assessment of their structural alignment with 4PD1.

### 2.2. Molecular Dynamics

Each of the five models was inserted into a heterogeneous neuronal plasma membrane (Table 1) using the CHARMM-GUI membrane builder [19,20]. A box of  $250 \text{ \AA} \times 250 \text{ \AA}$  was established with periodic boundary conditions. The system was solvated with 150 mM NaCl at a net charge of zero using the TIP3P water model [21]. The simulations were run in GROMACS [22] using the University of Cambridge High Performance Computing Resources. Long-range electrostatic interactions were calculated using the Particle-mesh Ewald method with the Coulomb and van der Waals interaction cut-offs set to  $12 \text{ \AA}$  [23]. The LINCS algorithm was used to constrain molecular bonds. All systems were run using the CHARMM36m force field. Following steepest descent minimisation, all systems were subjected to six series of a 125 picosecond NPT equilibration ensemble with temperature coupling with velocity rescaling and pressure coupling using the Parrinello–Rahman method [24–26] for all simulations. Simulation time steps were set at 2 fs, and, as RMSDs plateaued within 10 ns for all models, total simulation runtimes were 50 ns (receptor models) or 25 ns (docked receptor models); simulations were run 3–5 times for each model.

**Table 1.** Lipid composition of the neuronal plasma membrane.

Lipid	% Upper Leaf	% Lower Leaf
Cholesterol	44	44
DPPC	13	6
POPC	21	10
DOPC	6	3
POPE	16	21
POPS	0	10
POPI	0	5
POPA	0	1
Total	100	100

### 2.3. Model Analysis

Visual analysis of GROMACS trajectories was performed using VMD 1.9.4 [27], and snapshots were prepared using PyMOL (The PyMOL Molecular Graphics System, Version 1.2r3pre, Schrödinger, LLC, New York, NY, USA). Snapshots of the ICD were taken from trajectories for each model after equilibration. Stabilising interactions were calculated with RING 3.0, a residue interaction network representation of residue contacts [28]. The

default RING 3.0 settings were used with distance thresholds for interactions set at 3.5 Å for hydrogen bonding, 4 Å for ionic, 5 Å for  $\pi$ -cation, 6.5 Å for  $\pi$ - $\pi$  stacking, 2.5 Å for disulphide, and 0.5 Å for van der Waals. RMSD calculations (Equation (1)) were performed with the gmx rms module using the initial structure as a reference.

$$\text{RMSD}(t) = \sqrt{\frac{1}{N} \sum_{i=1}^N (r_i(t) - r_i^{\text{ref}})^2} \quad (1)$$

where  $N$  is the number of atoms in the model,  $t$  is the simulation timepoint,  $r_i$  is the set of coordinates of an atom, and  $r_i^{\text{ref}}$  is the set of coordinates of the same atom in the reference structure.

RMSF ( $\rho$ ) calculations (Equation (2)) were performed using the gmx rmsf module on C $\alpha$  atoms in the models. Average coordinates were calculated when the trajectory equilibrated as determined by RMSD values (10 ns—end for all trajectories).

$$\rho_i = \sqrt{\langle (r_i - \langle r_i \rangle)^2 \rangle} \quad (2)$$

where  $\rho_i$  is RMSF for an atom,  $r_i$  is the set of coordinates of that atom, and  $\langle r_i \rangle$  is the average set of coordinates of that atom.

Polar contacts between GephE and the GlyR  $\beta$  subunit in the docked models were determined by distance. Data were plotted using RStudio v1.3.1903 (RStudio Team (2020). RStudio: Integrated Development for R. RStudio, PBC, Boston, MA, USA URL <http://www.rstudio.com/> accessed on 10 March 2023).

#### 2.4. Statistics

RMSF data were transformed using a one-parameter Box–Cox power transformation [29] due to a lack of normality violating an assumption of ANOVA.

The transformation involves forming  $n$  pairs of sorted data and normalised data (Equation (3)). The value  $\lambda$ , which gives the greatest correlation between the pairs, was then used for the transformation. Data were then transformed using Equation (4).

$$\left( \Phi^{-1} \left( \frac{i - 0.5}{n} \right), x_{(i)} \right), \text{ for } i = 1, 2, \dots, n \quad (3)$$

where  $\Phi^{-1}$  is the inverse normal cumulative density function, and  $x_{(i)}$  is the  $i$ th sorted value.

$$x_i^\lambda = \begin{cases} \frac{x_i^\lambda - 1}{\lambda} & \text{if } \lambda \neq 0, \\ \ln(x_i) & \text{if } \lambda = 0 \end{cases} \quad (4)$$

Standard one-way ANOVA and Tukey Honestly Significant Difference tests were performed on transformed RMSF data.

Other data were compared using Student's test;  $p < 0.05$  was taken as significantly different.

### 3. Results

#### 3.1. GlyR Models

The GlyR models (Figure 2) show the ECDs and TMDs are similarly structured, while the ICD varies considerably; this is consistent with minimal flexibility in the ECD and TMD but a highly dynamic ICD. Nevertheless, the ICDs of all subunits in each model contained two short helices at the N and C termini, which we call hN and hC: AVNFSR ( $\alpha_1$  and  $\alpha_2$ , hN), KLFIQRAKKIDK ( $\alpha_1$ , hC), KfvRAKRIDT ( $\alpha_2$ , hC), VVQVMLNN ( $\beta$ , hN), and PVIPTAAKRIDL ( $\beta$ , hC).

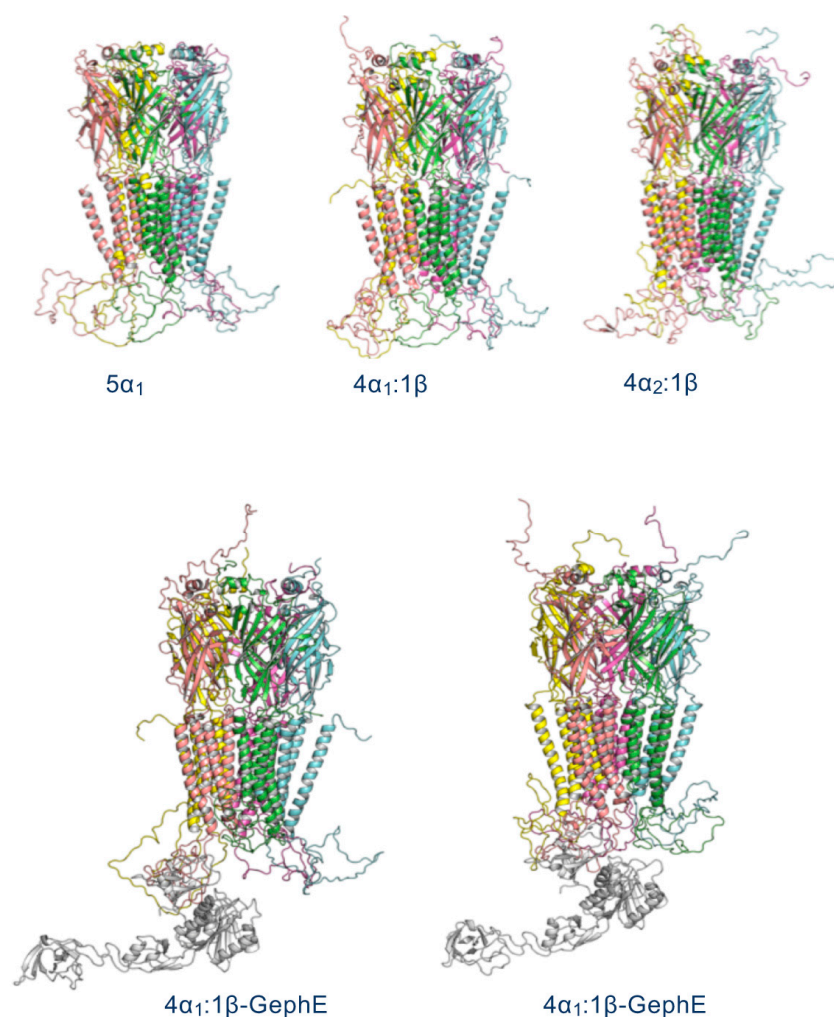


**Figure 2.** GlyR models. Colours distinguish subunits, with light pink (leftmost subunit) representing  $\beta$  in heteromeric models.

### 3.2. ICD Structure following MD Simulation

Visualisation of the MD trajectories identified a compaction of the ICDs over time (Figure 3). ICD compaction was most pronounced in the  $5\alpha_1$  model (its maximum width was reduced from  $115 \pm 8 \text{ \AA}$  to  $69 \pm 4 \text{ \AA}$ , mean  $\pm$  SEM,  $n = 3$ ), perhaps due to its initial pseudosymmetry and the absence of the larger  $\beta$  subunit ICD. The  $4\alpha_2:1\beta$  ICD underwent less compaction, but it also had the smallest diameter in its 0 ns structure. Pore diameter was not affected in any of the models and was relatively constant at  $\sim 30 \text{ \AA}$ .

The MD data also revealed that various secondary structures formed transiently, e.g., in the  $\beta$  subunit of the  $4\alpha_1:1\beta$  GlyR, a coil observed at  $^{421}\text{SIV}^{423}$  in the initial structure was lost over the trajectory, while in the  $\beta$  subunit of  $4\alpha_2:1\beta$  GlyR, a small helix was formed after 50 ns at  $^{406}\text{KKVCT}^{410}$ , as was a tripeptide  $\beta$  sheet at  $^{411}\text{SKS}^{413-423}\text{VIS}^{421}$ .

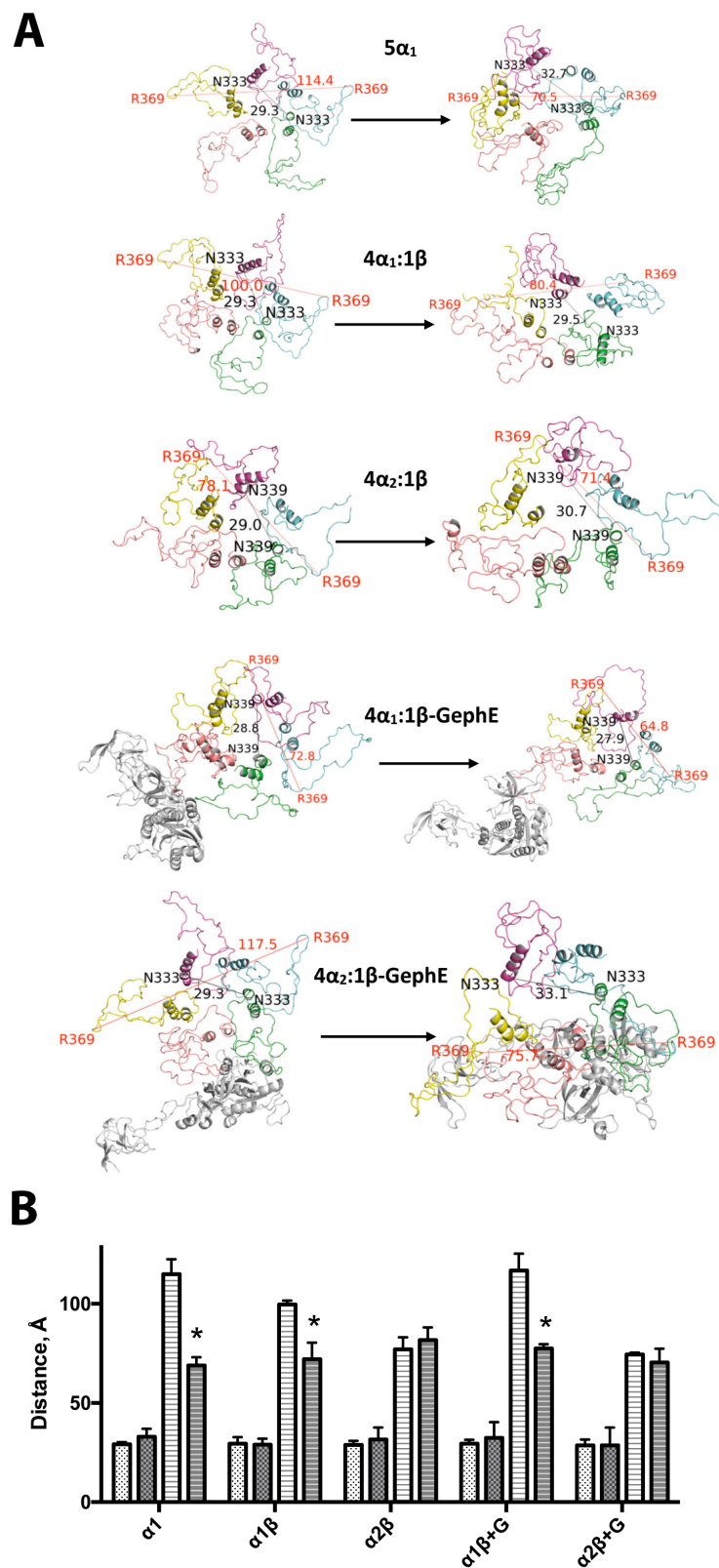


**Figure 3.** Changes in ICD structures after MD simulations. (A) Example structures from before (left-hand side) and after (right-hand side) the simulation, viewed from the bottom of the receptor. Typical of 3–5 production runs. The maximal ICD width (measured between C $\alpha$  in Å) is labelled in red, and the pore diameter (between C $\alpha$  in Å) in black. (B) Pore (spots) and diameter (lines) distances before (white) and after (grey) the MD simulations. \* = significantly different, Student’s *t* test, *p* < 0.05. Data = mean  $\pm$  SEM, *n* = 3.

### 3.3. ICD Interactions

Interactions that could stabilise the ICD were explored during the MD simulation for each model (Figure 4). These were predominantly van der Waals interactions and hydrogen bonds. For the unbound models, these increased during the simulation, but there was no increase in the docked models  $4\alpha_1:1\beta$ -GephE and  $4\alpha_2:1\beta$ -GephE. Given the paucity of data on pLGIC ICDs, it is not yet clear which interactions are likely to predominate in stabilising intracellular loops. These data do, however, suggest that the presence of GephE could stabilise the whole ICD.

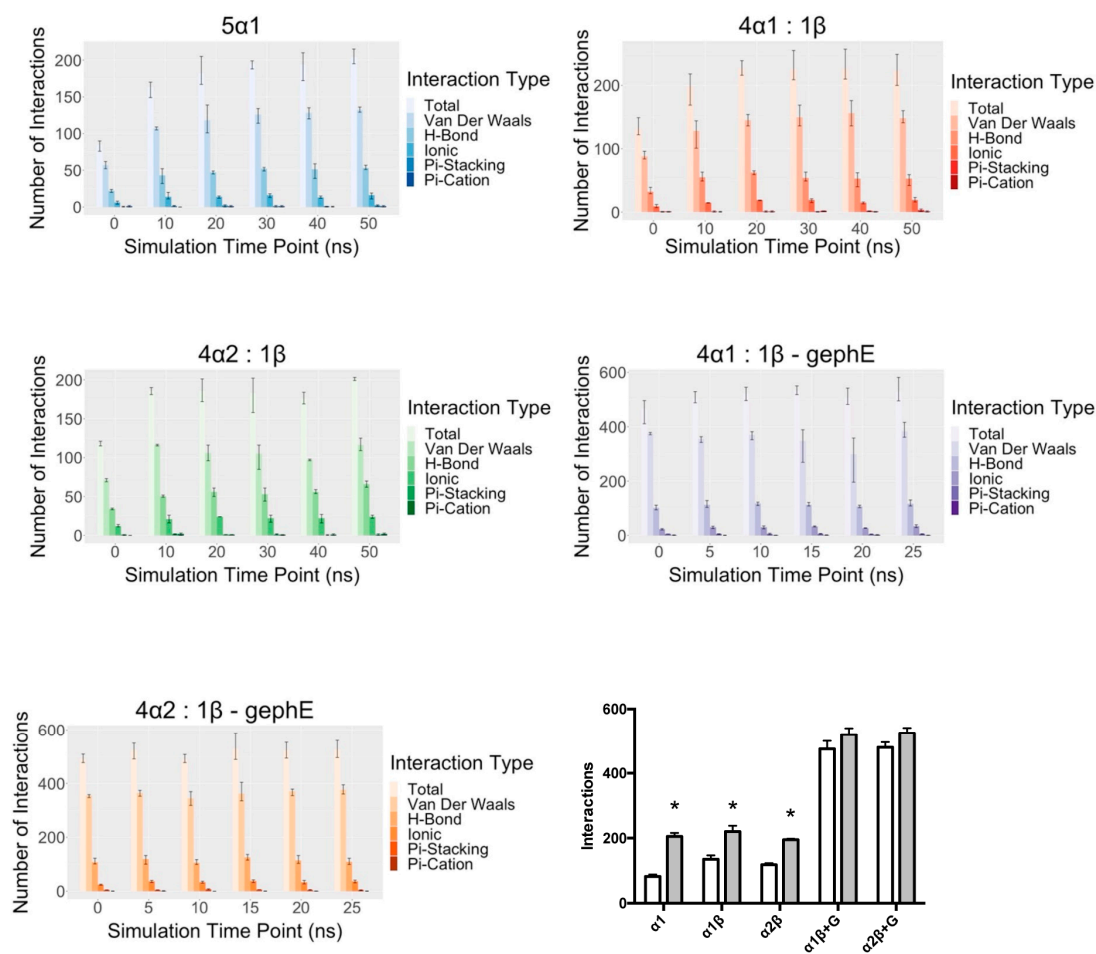


**Figure 4.** Changes in ICD interactions during the MD simulation for each model. A range of different interactions were identified and are shown in different shades of colour. For the unbound GlyR models ( $5\alpha_1$ ,  $4\alpha_2:1\beta$ , and  $4\alpha_2:1\beta$ ), the number of interactions increased during the simulation, but there was no significant increase in interactions in the bound models ( $4\alpha_1:1\beta$ -gephE and  $4\alpha_2:1\beta$ -gephE). This can be seen in the plot at the bottom right-hand side, which shows the total number of interactions at the start (white) and end (grey) of the simulations. \* = significantly different to start, Student's t test,  $p < 0.05$ . Data = mean  $\pm$  SEM,  $n = 3$ .

### 3.4. ICD $\beta$ Subunit Flexibility

The RMSF data showed that the  $\alpha$  subunit influenced the flexibility of the  $\beta$  subunit ICD: The  $\beta$  ICD in  $4\alpha_2:1\beta$  GlyR had a significantly larger RMSF, indicating greater flexibility in the  $\beta$  ICD here compared to the  $4\alpha_1:1\beta$  GlyR (Figure 5).

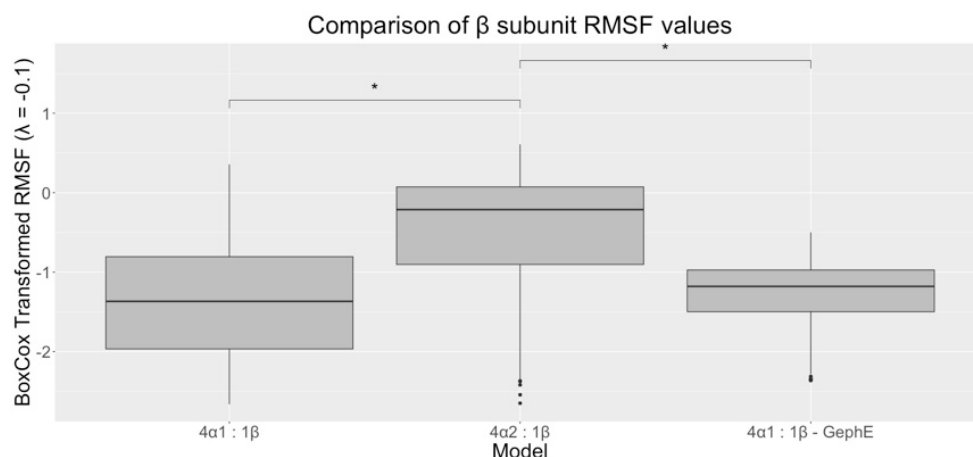


**Figure 5.** Comparison of Box–Cox transformed  $\beta$  subunit ICD RMSF values. The  $4\alpha_2:1\beta$  GlyR model had a larger RMSF value than  $4\alpha_1:1\beta$  and  $4\alpha_1:1\beta$ -GephE GlyRs. \* = significantly different at  $p < 0.0001$ ,  $n = 3$ .

### 3.5. Effects of GephE Binding on ICD Structure and Stability

GephE binding did not change the ICD pore diameters, which were  $29.5 \pm 0.6 \text{ \AA}$  versus  $29.9 \pm 0.5 \text{ \AA}$  for  $4\alpha_1:1\beta$  and  $4\alpha_1:1\beta$ -GephE respectively, and  $29.1 \pm 0.3 \text{ \AA}$  versus  $28.6 \pm 0.5 \text{ \AA}$  for  $4\alpha_2:1\beta$  and  $4\alpha_2:1\beta$ -GephE (data = mean  $\pm$  SEM,  $n = 3$ ). GephE binding did, however, reduce the maximum ICD width in the  $4\alpha_2:1\beta$  GlyR, which decreased from  $120.9 \pm 5.1 \text{ \AA}$  to  $86.7 \pm 4.1 \text{ \AA}$  (significantly different  $p < 0.01$ ). Width values for the  $4\alpha_1:1\beta$  GlyR were not significantly different ( $81.2 \pm 21 \text{ \AA}$  and  $78.7 \pm 22 \text{ \AA}$  with and without GephE, respectively), but observation of the bound models did reveal compaction (Figure 6); the diameter measurements did not reflect this as one loop of one  $\alpha_1$  subunit was extended despite the compaction of the other four subunits. Thus, the changes in structure were quite different for the two heteromeric receptors, illustrating that subtle differences in the binding of the same molecule to the same subunit in similar receptors could have very different outcomes.

A closer examination of the site of interaction between GlyR and GephE revealed that the  $4\alpha_2:1\beta$ -GephE binding site has more possible interactions than the  $4\alpha_1:1\beta$ -GephE binding site (Figure 7), thus hinting at the fact that there could be differences in affinity for gephyrin in the different heteromers.

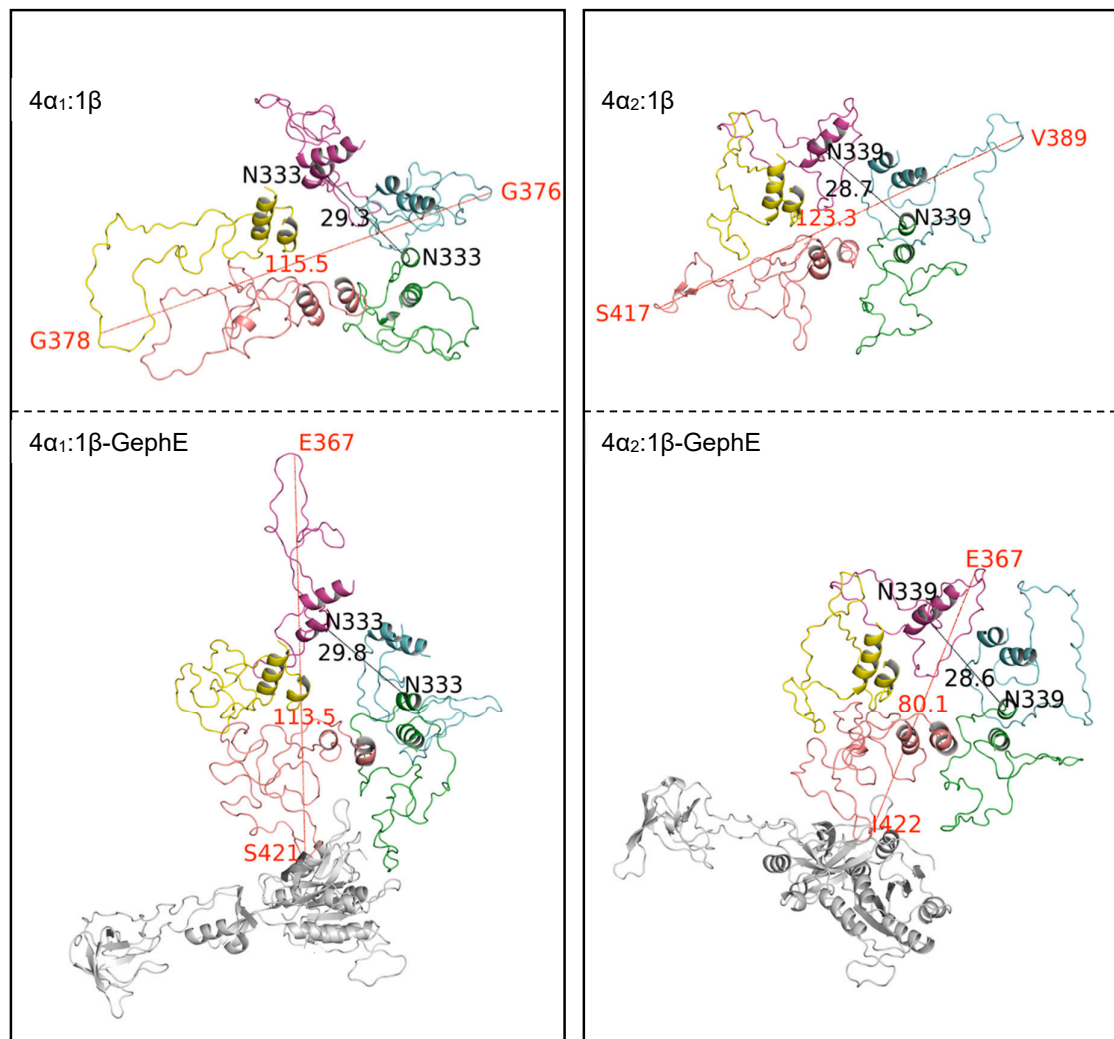


**Figure 6.** The effect of GephE binding on ICD structure. Images of ICDs without (upper panel) and with (lower panel) bound GephE. Typical of 3 production runs. Maximal ICD width (red) and pore diameter (black) in Å are shown.

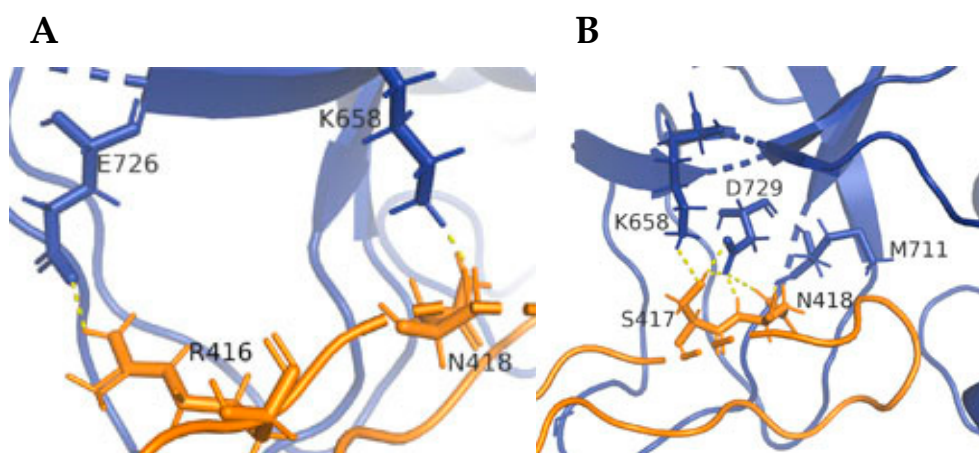


**Figure 7.** Residues involved in GephE binding may differ for  $4\alpha_1:1\beta$ -GephE (A) and  $4\alpha_2:1\beta$ -GephE (B). Potential interactions between gephyrin (blue) and the  $\alpha$  subunit (orange) following a typical MD production run are shown as dashed yellow lines. More potential interactions are observed in the  $4\alpha_2:1\beta$ -GephE model.

#### 4. Discussion

This study provides a predictive insight into the previously unknown structure and characteristics of the GlyR ICD and also shows that the ICD has the potential to undergo considerable conformational changes upon the binding of physiologically relevant intracellular proteins such as gephyrin. Structural studies to date have not been able to generate high-resolution structural details of this domain, but using molecular details from a related protein and the power of modelling and molecular dynamics, we have produced what is likely to be a reasonably, if not fully, accurate structure of the GlyR ICD.

The details revealed by our GlyR models explain why this region has proved intractable to structural experiments: much of it comprises a highly flexible loop, and this, combined with its considerable size and variability, is not conducive to obtaining good experimental data from classic structural techniques such as X-ray crystallography, cryo-electron microscopy and NMR. Computer-based studies are the only practical route to obtaining molecular information, and in using these, we observed a range of useful structural details. These include the fact that the ICDs of both  $\alpha$  and  $\beta$  subunits form helices at their N and C ends, and the flexible loop between these helices can support transient secondary structures. We show that there is greater flexibility of the  $\beta$  subunit in the  $4\alpha_2:1\beta$  GlyR compared to the  $4\alpha_1:1\beta$  GlyR, which suggests the possibility of different binding partners of the  $\beta$  subunit depending on the other receptor subunits. In addition, our data predict the effect and molecular details of gephyrin binding to the GlyR ICD. In our GephE-bound GlyRs, the ICDs are more compact, and the number of potential residue interactions between GephE and the  $\beta$  subunit differ in the  $4\alpha_2:1\beta$  GlyR compared to the  $4\alpha_1:1\beta$  GlyR. Thus, not only do our data suggest that the  $\beta$  subunit could have different binding partners depending on the  $\alpha$  subunits but also that the same binding partner could generate different conformational changes in different heteromers. The resulting different functional effects could help explain the reasons behind the differential expression of GlyR subunits in different tissues and over developmental timescales [30,31].

Our ICD models are broadly similar to the structure of the ICD of the  $\alpha_7$  nAChR ICD, which has recently been investigated [32]. However, when compared to the results presented here, the  $\alpha_7$  nAChR ICD has additional secondary structures: each subunit contains one C-terminal MA helix, one N-terminal MX helix, and three short helices (h1–h3). The h3 helix anchors the MA helix, resulting in a B-shaped architecture. We did find C-terminal and N-terminal helices in the GlyR ICD, but these were much shorter than the MA and MX helices. We did not observe any consistent helices equivalent to h1–h3 in the GlyR ICD, although analysis using the secondary-structure prediction program PSIPRED [33] did predict a number of short helices and strands which largely occurred in positions similar to the transient secondary structures we observed. Thus, our data suggest that GlyR ICDs are more disordered than those of  $\alpha_7$  nAChR, with fewer fixed secondary structures.

Disorder is likely to be an important feature of Cys-loop receptor ICDs. Disorder is known to be prevalent across eukaryotic proteins, particularly signalling proteins [34,35], and it may provide an evolutionary advantage by allowing binding to a wide variety of partners [36]. To date, four intracellular binding partners of GlyR ICDs have been identified: gephyrin, neurobeachin, vacuolar protein sorting 35, and syndapin I [37–39]. All of these proteins bind to the  $\beta$  subunit in the ICD, with only one—syndapin I—also binding to the  $\alpha$  subunit. Binding to disordered regions often induces a conformational change [40], and we propose that this would be the case when these partners bind to the GlyR ICD. This hypothesis is supported by our models, which show ICD compaction when GephE is bound. A conformational change in the ICD could also affect other regions of the protein, causing changes to the function and/or interactions of the receptor.

All the results presented here were generated using a computational approach involving *ab initio* model generation and MD simulations. There are still a number of well-recorded potential errors in these and related software programs, which have particular difficulty in generating multimeric proteins and loop regions [41,42]. Nevertheless,

in silico approaches have proved useful and are continually improving; not only have they led to increasingly accurate predictions, but they are often the only practical route to obtaining data. Here, an in silico method was necessary due to the size and intrinsic disorder of GlyR ICDs, which have largely prevented experimentally solved structures from being useful; some previous experimental attempts have, for example, resulted in low-resolution “blob-ology” [6]. Our models and simulations are therefore useful in creating hypotheses which can be further tested, and they provide a starting point for future research and development.

## 5. Conclusions

In conclusion, this study reveals likely features of the previously unknown structure, stability, and flexibility of the GlyR ICD. As no structures of this region in the GlyR are currently available, we used a bioinformatic approach to generate plausible models of the ICDs of three different GlyRs: one homomeric receptor ( $5\alpha_1$ ) and two heteromeric receptors ( $4\alpha_1:1\beta$  and  $4\alpha_2:1\beta$ ). These were then subjected to MD simulations to improve accuracy. The outputs revealed more compact structures than our initial models suggested, with an increased number of intracellular interactions. Our data also indicated that the type of  $\alpha$  subunit could influence the flexibility of the  $\beta$  subunit, with the  $\beta$  subunit ICD in  $4\alpha_2:1\beta$  receptors likely having greater flexibility compared to the  $4\alpha_1:1\beta$  GlyR. This structural diversity of GlyR ICDs may be related to the functional diversity of different GlyR isoforms.

We also generated two models of GlyRs bound to gephyrin. Gephyrin is an intracellular protein and has been well documented as a GlyR-binding protein which controls receptor localisation and clustering. It has three important domains: a C domain, an E domain, and a G domain. The C domain is important for localisation, as it binds to microtubules, while the E and G domains are important for clustering: the E domain can dimerise and the G domain can trimerise. These gephyrin oligomerisations via the E and/or G domains cause GlyR clustering through the formation of sub-membranous, hexagonal lattices. Gephyrin binds to GlyR  $\beta$  subunits; molecular details of this have been revealed from a crystal structure of a 15-amino-acid  $\beta$  subunit peptide from gephyrin bound to GlyRs via its E domain [10]. We used these data to help generate two models of the GlyR bound to Geph.:  $4\alpha_1:1\beta$ -GephE and  $4\alpha_2:1\beta$ -GephE. MD simulations of these models revealed no increase in total ICD binding interactions, indicating that GephE had sufficiently stabilised the original structures. However, a visual inspection revealed that the bound GlyR was more compact in at least four of its five subunits. There was also evidence that the different  $\alpha$  subunits influence the binding differently: the  $4\alpha_2:1\beta$  GlyR-GephE binding site has more potential interactions than the  $4\alpha_1:1\beta$  GlyR-GephE binding site, indicating possible different affinities for gephyrin in the different heteromers. Differences in receptor compaction and binding affinity could be transduced to other regions of the receptor to generate different functional effects.

Thus, overall, our study has enhanced our knowledge of the structure and interactions of the GlyR and revealed a range of features that could explain its different functions, especially those that involve binding to its best-studied interaction partner, gephyrin.

**Author Contributions:** Conceptualisation, all authors; experimental investigation, J.R.E.T. and C.A.B.; data analysis, J.R.E.T., S.C.R.L. and C.A.B.; writing—all authors; project administration, S.C.R.L. All authors have read and agreed to the published version of the manuscript.

**Funding:** S.C.R.L. was supported by the M.R.C. (MRL021676/1).

**Data Availability Statement:** Data are available on request from the authors.

**Conflicts of Interest:** The authors declare no conflict of interest.

## References

1. Rajendra, S.; Lynch, J.W.; Schofield, P.R. The glycine receptor. *Pharmacol. Ther.* **1997**, *73*, 121–146. [[CrossRef](#)] [[PubMed](#)]
2. Thompson, A.J.; Lester, H.A.; Lummis, S.C. The structural basis of function in Cys-loop receptors. *Q. Rev. Biophys.* **2010**, *43*, 449–499. [[CrossRef](#)] [[PubMed](#)]

3. Harvey, R.J.; Depner, U.B.; Wassele, H.; Ahmadi, S.; Heindl, C.; Reinold, H.; Smart, T.G.; Harvey, K.; Schutz, B.; Abo-Salem, O.M.; et al. GlyR alpha3: An essential target for spinal PGE2-mediated inflammatory pain sensitization. *Science* **2004**, *304*, 884–887. [[CrossRef](#)] [[PubMed](#)]
4. Rees, M.I.; Harvey, K.; Ward, H.; White, J.H.; Evans, L.; Duguid, I.C.; Hsu, C.C.; Coleman, S.L.; Miller, J.; Baer, K.; et al. Isoform heterogeneity of the human gephyrin gene (GPHN), binding domains to the glycine receptor, and mutation analysis in hyperekplexia. *J. Biol. Chem.* **2003**, *278*, 24688–24696. [[CrossRef](#)] [[PubMed](#)]
5. Shiang, R.; Ryan, S.G.; Zhu, Y.Z.; Hahn, A.F.; O’Connell, P.; Wasmuth, J.J. Mutations in the alpha 1 subunit of the inhibitory glycine receptor cause the dominant neurologic disorder, hyperekplexia. *Nat. Genet.* **1993**, *5*, 351–358. [[CrossRef](#)]
6. Zhu, H.; Gouaux, E. Architecture and assembly mechanism of native glycine receptors. *Nature* **2021**, *599*, 513–517. [[CrossRef](#)] [[PubMed](#)]
7. Yu, H.; Bai, X.C.; Wang, W. Characterization of the subunit composition and structure of adult human glycine receptors. *Neuron* **2021**, *109*, 2707–2716.e6. [[CrossRef](#)]
8. Sola, M.; Bavro, V.N.; Timmins, J.; Franz, T.; Ricard-Blum, S.; Schoehn, G.; Ruigrok, R.W.; Paarmann, I.; Saiyed, T.; O’Sullivan, G.A.; et al. Structural basis of dynamic glycine receptor clustering by gephyrin. *EMBO J.* **2004**, *23*, 2510–2519. [[CrossRef](#)]
9. Tyagarajan, S.K.; Fritschy, J.M. Gephyrin: A master regulator of neuronal function? *Nat. Rev. Neurosci.* **2014**, *15*, 141–156. [[CrossRef](#)]
10. Maric, H.M.; Kasaragod, V.B.; Schindelin, H. Modulation of gephyrin-glycine receptor affinity by multivalency. *ACS Chem. Biol.* **2014**, *9*, 2554–2562. [[CrossRef](#)]
11. Ivica, J.; Lape, R.; Jazbec, V.; Yu, J.; Zhu, H.; Gouaux, E.; Gold, M.G.; Sivilotti, L.G. The intracellular domain of homomeric glycine receptors modulates agonist efficacy. *J. Biol. Chem.* **2021**, *296*, 100387. [[CrossRef](#)] [[PubMed](#)]
12. Moraga-Cid, G.; San Martin, V.P.; Lara, C.O.; Munoz, B.; Marileo, A.M.; Sazo, A.; Munoz-Montesino, C.; Fuentealba, J.; Castro, P.A.; Guzman, L.; et al. Modulation of glycine receptor single-channel conductance by intracellular phosphorylation. *Sci. Rep.* **2020**, *10*, 4804. [[CrossRef](#)] [[PubMed](#)]
13. Torres, P.H.M.; Rossi, A.D.; Blundell, T.L. ProtCHOIR: A tool for proteome-scale generation of homo-oligomers. *Brief. Bioinform.* **2021**, *22*, bbab182. [[CrossRef](#)] [[PubMed](#)]
14. Sali, A.; Blundell, T.L. Comparative protein modelling by satisfaction of spatial restraints. *J. Mol. Biol.* **1993**, *234*, 779–815. [[CrossRef](#)] [[PubMed](#)]
15. Huang, X.; Chen, H.; Michelsen, K.; Schneider, S.; Shaffer, P.L. Crystal structure of human glycine receptor-alpha3 bound to antagonist strychnine. *Nature* **2015**, *526*, 277–280. [[CrossRef](#)] [[PubMed](#)]
16. Katoh, K.; Standley, D.M. MAFFT multiple sequence alignment software version 7: Improvements in performance and usability. *Mol. Biol. Evol.* **2013**, *30*, 772–780. [[CrossRef](#)] [[PubMed](#)]
17. Jumper, J.; Evans, R.; Pritzel, A.; Green, T.; Figurnov, M.; Ronneberger, O.; Tunyasuvunakool, K.; Bates, R.; Zidek, A.; Potapenko, A.; et al. Highly accurate protein structure prediction with AlphaFold. *Nature* **2021**, *596*, 583–589. [[CrossRef](#)]
18. Chen, R.; Weng, Z. Docking unbound proteins using shape complementarity, desolvation, and electrostatics. *Proteins* **2002**, *47*, 281–294. [[CrossRef](#)]
19. Jo, S.; Kim, T.; Iyer, V.G.; Im, W. CHARMM-GUI: A web-based graphical user interface for CHARMM. *J. Comput. Chem.* **2008**, *29*, 1859–1865. [[CrossRef](#)]
20. Lee, J.; Cheng, X.; Swails, J.M.; Yeom, M.S.; Eastman, P.K.; Lemkul, J.A.; Wei, S.; Buckner, J.; Jeong, J.C.; Qi, Y.; et al. CHARMM-GUI Input Generator for NAMD, GROMACS, AMBER, OpenMM, and CHARMM/OpenMM Simulations Using the CHARMM36 Additive Force Field. *J. Chem. Theory Comput.* **2016**, *12*, 405–413. [[CrossRef](#)]
21. Joung, I.S.; Cheatham, T.E., III. Determination of alkali and halide monovalent ion parameters for use in explicitly solvated biomolecular simulations. *J. Phys. Chem. B* **2008**, *112*, 9020–9041. [[CrossRef](#)]
22. Abraham, M.J.; Murtola, T.; Schulz, R.; Pall, S.; Smith, J.C.; Hess, B.; Lindahl, E. GROMACS: High performance molecular simulations through multi-level parallelism from laptops to supercomputers. *SoftwareX* **2015**, *1*, 19–25. [[CrossRef](#)]
23. Darden, T.; York, D.; Pedersen, L. Particle mesh Ewald: An N·log(N) method for Ewald sums in large systems. *J. Chem. Phys.* **1993**, *98*, 10089–10092. [[CrossRef](#)]
24. Huang, J.; Rauscher, S.; Nawrocki, G.; Ran, T.; Feig, M.; de Groot, B.L.; Grubmuller, H.; MacKerell, A.D., Jr. CHARMM36m: An improved force field for folded and intrinsically disordered proteins. *Nat. Methods* **2017**, *14*, 71–73. [[CrossRef](#)] [[PubMed](#)]
25. Bussi, G.; Donadio, D.; Parrinello, M. Canonical sampling through velocity rescaling. *J. Chem. Phys.* **2007**, *126*, 014101. [[CrossRef](#)] [[PubMed](#)]
26. Parrinello, M.; Rahman, A. Polymorphic transitions in single crystals: A new molecular dynamics method. *J. Appl. Phys.* **1981**, *52*, 7182–7190. [[CrossRef](#)]
27. Humphrey, W.; Dalke, A.; Schulten, K. VMD: Visual molecular dynamics. *J. Mol. Graph.* **1996**, *14*, 33–38. [[CrossRef](#)]
28. Clementel, D.; Del Conte, A.; Monzon, A.M.; Camagni, G.F.; Minervini, G.; Piovesan, D.; Tosatto, S.C.E. RING 3.0: Fast generation of probabilistic residue interaction networks from structural ensembles. *Nucleic Acids Res.* **2022**, *50*, W651–W656. [[CrossRef](#)]
29. Box, G.E.P.; Cox, D.R. An analysis of transformations (with discussion). *J. R. Stat. Soc. B* **1964**, *26*, 211–252.
30. Delaney, A.J.; Esmaili, A.; Sedlak, P.L.; Lynch, J.W.; Sah, P. Differential expression of glycine receptor subunits in the rat basolateral and central amygdala. *Neurosci. Lett.* **2010**, *469*, 237–242. [[CrossRef](#)]

31. Malosio, M.L.; Marqueze-Pouey, B.; Kuhse, J.; Betz, H. Widespread expression of glycine receptor subunit mRNAs in the adult and developing rat brain. *EMBO J.* **1991**, *10*, 2401–2409. [[CrossRef](#)]
32. Bondarenko, V.; Wells, M.M.; Chen, Q.; Tillman, T.S.; Singewald, K.; Lawless, M.J.; Caporoso, J.; Brandon, N.; Coleman, J.A.; Saxena, S.; et al. Structures of highly flexible intracellular domain of human alpha7 nicotinic acetylcholine receptor. *Nat. Commun.* **2022**, *13*, 793. [[CrossRef](#)]
33. McGuffin, L.J.; Bryson, K.; Jones, D.T. The PSIPRED protein structure prediction server. *Bioinformatics* **2000**, *16*, 404–405. [[CrossRef](#)] [[PubMed](#)]
34. Iakoucheva, L.M.; Brown, C.J.; Lawson, J.D.; Obradovic, Z.; Dunker, A.K. Intrinsic disorder in cell-signaling and cancer-associated proteins. *J. Mol. Biol.* **2002**, *323*, 573–584. [[CrossRef](#)] [[PubMed](#)]
35. Ward, J.J.; Sodhi, J.S.; McGuffin, L.J.; Buxton, B.F.; Jones, D.T. Prediction and functional analysis of native disorder in proteins from the three kingdoms of life. *J. Mol. Biol.* **2004**, *337*, 635–645. [[CrossRef](#)] [[PubMed](#)]
36. Wright, P.E.; Dyson, H.J. Intrinsically disordered proteins in cellular signalling and regulation. *Nat. Rev. Mol. Cell Biol.* **2015**, *16*, 18–29. [[CrossRef](#)] [[PubMed](#)]
37. Prior, P.; Schmitt, B.; Grenningloh, G.; Pribilla, I.; Multhaup, G.; Beyreuther, K.; Maulet, Y.; Werner, P.; Langosch, D.; Kirsch, J.; et al. Primary structure and alternative splice variants of gephyrin, a putative glycine receptor-tubulin linker protein. *Neuron* **1992**, *8*, 1161–1170. [[CrossRef](#)]
38. del Pino, I.; Paarmann, I.; Karas, M.; Kilimann, M.W.; Betz, H. The trafficking proteins Vacuolar Protein Sorting 35 and Neurobeachin interact with the glycine receptor beta-subunit. *Biochem. Biophys. Res. Commun.* **2011**, *412*, 435–440. [[CrossRef](#)]
39. Del Pino, I.; Koch, D.; Schemm, R.; Qualmann, B.; Betz, H.; Paarmann, I. Proteomic analysis of glycine receptor beta subunit (GlyRbeta)-interacting proteins: Evidence for syndapin I regulating synaptic glycine receptors. *J. Biol. Chem.* **2014**, *289*, 11396–11409. [[CrossRef](#)]
40. Meszaros, B.; Simon, I.; Dosztanyi, Z. Prediction of protein binding regions in disordered proteins. *PLoS Comput. Biol.* **2009**, *5*, e1000376. [[CrossRef](#)]
41. Barozet, A.; Chacon, P.; Cortes, J. Current approaches to flexible loop modeling. *Curr. Res. Struct. Biol.* **2021**, *3*, 187–191. [[CrossRef](#)] [[PubMed](#)]
42. Evans, R.; O'Neill, M.; Protzel, A.; Antropova, N.; Senior, A.; Green, T.; Zidek, A.; Bates, R.; Blackwell, S.; Yim, J.; et al. Protein complex prediction with AlphaFold-Multimer. *bioRxiv* **2021**.

**Disclaimer/Publisher's Note:** The statements, opinions and data contained in all publications are solely those of the individual author(s) and contributor(s) and not of MDPI and/or the editor(s). MDPI and/or the editor(s) disclaim responsibility for any injury to people or property resulting from any ideas, methods, instructions or products referred to in the content.